A Simplified Mechanical Model for Rocking Structures on Compliant Foundations

Baojun Yuan * , Mirjam Kloos , Hamid Sadegh-Azar

Posted Date: 18 March 2026

doi: 10.20944/preprints202603.1401.v1

Keywords: soil-structure interaction (SSI); rocking dynamics; lagrange equation; compliant foundation

 doi:10.20944/preprints202603.1401.v1

Article

A Simplified Mechanical Model for Rocking Structures on Compliant Foundations

Baojun Yuan [1,*], Mirjam Kloos [2] and Hamid Sadegh-Azar [3]

[1] Institute of Structural Analysis and Dynamics, Department of civil engineering, RPTU University Kaiserslautern-Landau

[2] KOCH Solution Gmbh

[3] Institute of Structural Analysis and Dynamics, Department of civil engineering, RPTU University Kaiserslautern-Landau

* Correspondence: baojun.yuan@bauing.uni-kl.de

Abstract

Housner's classical rocking model assumes a rigid base, often leading to inaccurate seismic assessments in real-world soil conditions. This study quantitatively establishes the applicability limits of the rigid-base assumption and defines a reference range for its validity. To bridge this gap, a novel Soil-Structure Interaction (SSI)-rocking model is formulated via the Lagrange Equation, capturing the coupled dynamics between rocking blocks and compliant foundations. Crucially, a closed-form relationship is derived to correlate the analytical model's interface stiffness with the shear and Young's moduli used in industrial finite element (FE) software. Our findings reveal that rocking behavior depends not only on soil stiffness but also on the inherent stiffness of the structure. Consequently, a relative stiffness parameter is introduced to bridge the analytical and numerical frameworks. Validation using LS-DYNA confirms the model's precision across varying base stiffnesses. Results indicate that softer soils significantly alter rocking initiation thresholds and amplify peak angles. This proposed analytical model provides a computationally efficient, FE-compatible tool to improve stability predictions and design strategies for unanchored structures in earthquake-prone regions.

Keywords: soil-structure interaction (SSI); rocking dynamics; lagrange equation; compliant foundation

1. Introduction

The seismic resilience of large mobile equipment, including cranes, stacker-reclaimers, and ship loaders, has garnered significant attention in recent years, driven by their increasing prevalence in seismically active regions [1–3]. Unlike conventional fixed structures, these non-anchored systems exhibit unique dynamic characteristics, notably their ability to uplift, tilt, and rock during seismic events. To effectively analyze this rocking behavior, idealizing the equipment as a rigid body provided a simplified yet representative approach. Pioneering work by Housner (1963) established the groundwork for understanding rocking response by examining the behavior of rigid blocks [4]. His research introduced fundamental concepts such as the critical acceleration required to initiate rocking while also revealing the highly nonlinear nature of rocking dynamics. This nonlinearity arose from energy dissipation through impacts and intricate interactions with the supporting ground, underscoring the complexity of accurately predicting the seismic response of such equipment.

Yim, Chopra, and Penzien (1980) extended the analysis to consider the effects of base flexibility, showing that a compliant foundation could significantly alter the rocking response [5]. Their work emphasized the importance of soil-structure interaction (SSI) in predicting the seismic performance of rocking blocks. Further research by Makris and Zhang (2001) investigated the influence of block geometry and aspect ratio on rocking stability [6]. They demonstrated that taller, slender blocks were

 doi:10.20944/preprints202603.1401.v1

more susceptible to overturning compared to shorter, wider blocks, providing valuable insights into the geometric parameters that affect the rocking dynamics. The role of damping was also scrutinized. ElGawady et al. (2011) conducted experimental tests on free-rocking blocks with different interface materials, showing that rubber interfaces exhibited the highest energy dissipation due to continuous damping mechanisms, while rigid interfaces like concrete and timber led to discrete energy dissipation patterns [7]. DeJong (2014) introduced the concept of dynamically equivalent rocking structures by deriving approximate equivalence between different rocking systems. The study proposed a local linearization approach to estimate errors in modeling multi-block rocking mechanisms, enabling improved seismic response predictions for complex rocking structures [8,9]. Another research team, Vassiliou et al., analyzed the rocking response of structures, focusing on solitary rocking bodies and their self-stabilization potential under seismic excitations [10]. They derived analytical solutions and explored dynamic characteristics to assess stability. Vassiliou et al. (2015, 2016) extended this work by developing analytical and finite element models to incorporate deformation effects in rocking blocks, improving seismic response prediction for both rigid and deformable structures [11,12].

Bachmann et al. (2017, 2019) investigated the dynamics of rocking and rolling structures, focusing on their predictability and response under seismic excitations. They analyzed podium structures and rigid uplifting systems, highlighting key parameters influencing stability and overturning mechanisms [13–15]. Lachanas et al. (2022) analyzed the influence of the vertical component of ground motion on rocking structures, showing that it significantly altered overturning probabilities and energy dissipation [16]. Reggiani Manzo et al. (2019, 2022) proposed displacement-based analysis methods and developed uniform risk spectra for rocking structures, providing a probabilistic framework to assess their seismic reliability [17,18]. Sieber et al. (2020) examined the robustness of simplified analysis methods for rocking structures, comparing them against detailed numerical simulations to identify limitations in existing predictive models [19]. Kazantzi et al. (2021) presented seismic response distribution expressions for rocking structures, offering probabilistic models for overturning risk assessment [20]. Lachanas et al. (2021, 2022) introduced rocking incremental dynamic analysis and statistical parameterization techniques to quantify rocking response variability under seismic excitation [21,22]. Their findings improved fragility assessment and performance-based seismic evaluation.

Beyond rocking on rigid foundations, recent studies explored how base compliance could critically alter the observed rocking response, necessitating more sophisticated analytical models. Palmeri et al. (2008) conducted response analysis of rigid structures rocking on flexible foundations, demonstrating how soil-structure interaction modified fundamental rocking behavior [23]. They proposed a simplified approach to account for base compliance in seismic assessments. Vassiliou et al. (2011) analyzed the rocking response of rigid blocks on an isolation base, concluding that seismic isolation removed the beneficial property of increasing stability as block size increased or excitation pulse period decreased [24]. Pelekis et al. (2018, 2019) investigated the seismic behavior of buildings with structural and foundation rocking, emphasizing the interaction between soil and rocking motion. They showed that the relative density of sand did not influence structural rocking. Buildings with structural rocking experienced reduced base shear and floor accelerations compared to fixed-base structures. Their findings emphasized that well-designed structural rocking could enhance seismic resilience by limiting inelastic deformations and reducing overall damage [25,26]. Lu et al. (2021) developed an improved Winkler-based rocking foundation model that incorporated biaxial hysteretic soil behavior to better capture rocking isolation effects. They found that sliding due to coupled shear-compressive soil behavior tended to reduce free-vibrational rocking response of blocks with smaller slenderness ratios, while it could either increase or decrease seismic overturning potential of blocks on heavily loaded foundations [27]. He et al. extended the rigid rocking block model with a Winkler foundation to consider the flexibility of the foundation [28]. The study found that damping enhanced overturning resistance, while soil stiffness significantly influenced taller structures. Frost et al. (2023) investigated the dynamic response of rectangular rigid blocks standing

 doi:10.20944/preprints202603.1401.v1

on a horizontally moving compliant base, combining analytical, numerical, and experimental approaches [29]. By modeling the impact between the block and the moving base with a series of springs and dampers, the study highlighted the enhanced predictive capabilities of the compliant base model over traditional rigid base models in predicting the initiation of rocking and overall seismic response.

While previous research primarily focused on rocking structures directly on a rigid base, the influence of soil compliance and damping on rocking behavior had been relatively less studied. To fill this gap, this research proposes a new integrated SSI-rocking model and investigates the applicability limits of the classical Housner rocking formulation when soil flexibility and damping are considered.

2. The Applicability Limits of Housner's Rocking Block Model

Housner's rocking block model (**Figure 1**) provides a fundamental framework for analyzing the seismic behavior of unanchored structures, assuming a rigid block on a perfectly rigid base where rocking occurs about fixed pivot points without sliding. The model neglects any internal deformation, treating the structure as a pure rigid body, and considers energy dissipation only through impact when the block switches pivot points. Overturning is defined by exceeding a critical rocking angle, determined by the block's geometry and seismic excitation, without accounting for foundation flexibility or soil damping effects. The angular rotation can be computed by solving nonlinear ordinary differential equations:

$$\ddot{\theta}(t) = -\rho^2\{\sin(\alpha \cdot \mathrm{sgn}(\theta(t)) - \theta(t)) + \frac{\ddot{u}_g(t)}{g}\cos(\alpha \cdot \mathrm{sgn}(\theta(t)) - \theta(t))\} \quad (1)$$

where α represents the slenderness angle of the block which was computed by width and length of the block:

$$\alpha = \tan^{-1}\left(\frac{b}{h}\right) \quad (2)$$

ρ is the frequency parameter of the rocking block:

$$\rho = \sqrt{\frac{3g}{4R}} \quad (3)$$

The condition to initiate rocking for the rigid block model id determined by the peak ground acceleration (PGA) threshold, where the horizontal ground acceleration exceeds the block's static stability limit.

$$a_g > g\tan\alpha \quad (4)$$

During pure rocking, where no sliding or bouncing occurs, the kinetic energy dissipates during each impact to the base. This kinetic energy loss can be treated with coefficient restitution. The relationship of the angular velocities before and after impact gives:

$$r = \frac{\dot{\theta}_2}{\dot{\theta}_1} \quad (5)$$

The formula, that defines the upper bound for the coefficient of restitution of a rigid rocking block, based on angular momentum conservation before and after impact, is given by [4]:

$$r = 1 - \frac{3}{2}sin^2(\alpha) \quad (6)$$

 doi:10.20944/preprints202603.1401.v1

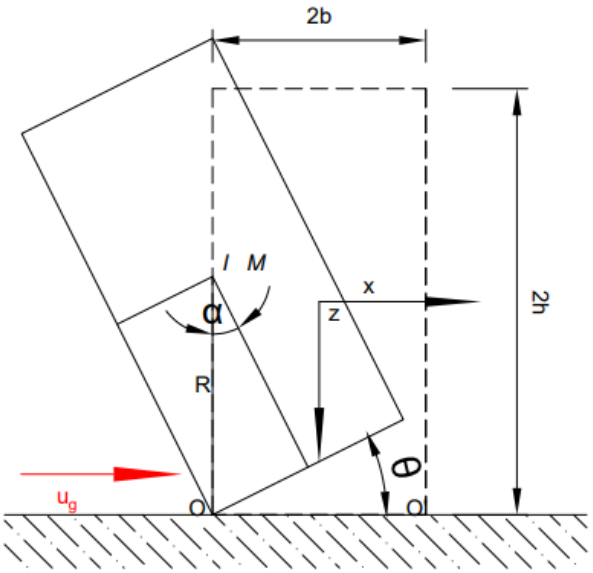

Figure 1. Housner's rocking block model.

The classical Housner rocking model, which neglects soil flexibility, was evaluated through detailed numerical simulations using the LS-DYNA explicit solver to explicitly model realistic base conditions and quantify the limitations of this simplification, while also assessing rocking motion and soil-structure interaction (SSI) under varying soil conditions. The numerical model, as depicted in **Figure 2**, provides a simplified two-dimensional representation of a block-soil system, designed for validation by comparing results against analytical predictions. This model comprises a rigid superstructure, represented by a red rectangular block symbolizing a non-building structure or column, and a blue rectangular base denoting the underlying soil or foundation. Both the block and soil components were modeled using elastic material properties. The rocking motion was simulated by implementing the keyword CONTACT_2D_AUTOMATIC_SURFACE_TO_SURFACE, enabling accurate representation of the dynamic interaction between the block and the base. To further delineate the applicability limits of the Housner model, a parametric study was performed by systematically varying the soil properties.

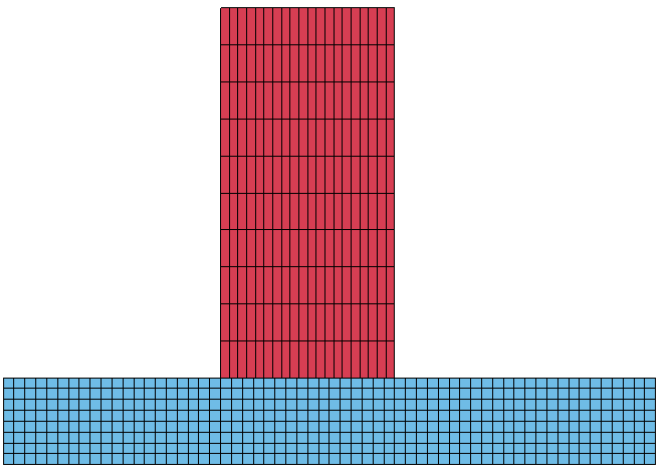

Figure 2. the numerical model in LS-DYNA.

The underlying soil was characterized by using representative soil parameters, including soil density ρ, shear modulus G_{max} and Poisson's ratio μ and dynamic stiffness modulus E_d, as

 doi:10.20944/preprints202603.1401.v1

summarized in **Table 1**. The relationship between dynamic shear modulus and dynamic elastic modulus is defined [30]:

$$E_d = G_d \frac{2(1-\mu)}{1-2\mu} \tag{7}$$

The selected soil ranged broadly from very soft (clay) to highly stiff (rock) and nearly rigid (steel) enabling a comprehensive assessment of soil compliance impacts on rocking behavior. For each soil configuration, the numerical rocking response of the rigid block under seismic loading was compared directly with the analytical solution from Housner's model. By evaluating discrepancies between results from numerical simulation and Housner's model, we clearly identified a critical stiffness threshold below which Housner's model predictions become unreliable. This threshold, defined by a shear modulus ranging from 300 to 1000 MPa.

Table 1. Soil properties for modelling compliant base.

Ground Type	Density ρ (kg/m^3)	Dynamic Shear Modulus G_{max} (MN/m^2)	Poisson's Ratio μ	Dynamic Elastic Modulus E_d (MN/m^2)
Sand	1900	80	0.3	280
Gravel	2000	300	0.3	1050
Rock	2500	1000	0.3	3500
Steel	7800	80000	0.3	210000

The subsequent investigation, underpinned by LS-DYNA simulations under both cosine function and earthquake excitation tests (as illustrated in **Figure 3**), revealed critical insights into the applicability of Housner's model. The model exhibited a relatively robust agreement with the predicted rocking motion on rigid bases, such as steel (E=210,000 MPa) and rock (G=1000 MPa). However, as the soil stiffness diminished, particularly when the shear modulus fell below 300 MPa, the Housner model's assumptions of a rigid base proved inadequate, rendering it inapplicable for accurately predicting rocking behavior on softer soil substrates. In addition, the maximal rocking angle increases sharply by soil type clay.

The criterion for initiating rocking motion is significantly altered when soil flexibility is considered, as demonstrated in **Figure 4** (4a, 4c,4e, 4g). While Housner's classical model predicts no rocking motion under cosine excitation due to its rigid-base assumption, the LS-DYNA simulations reveal that rocking is indeed initiated, driven by the compliant nature of the soil base. Moreover, the simulations indicate that the softer the soil, the larger the rocking motion could become, owing to increased base compliance and reduced effective stiffness. This phenomenon is also presented in **Figure 4** (4b, 4d, 4f, 4h). This discrepancy underscores the limitations of Housner's formulation in capturing soil-structure interaction effects, highlighting the imperative need to develop an enhanced rocking model that explicitly accounts for the dynamics of a compliant base to accurately predict rocking behavior under such conditions.

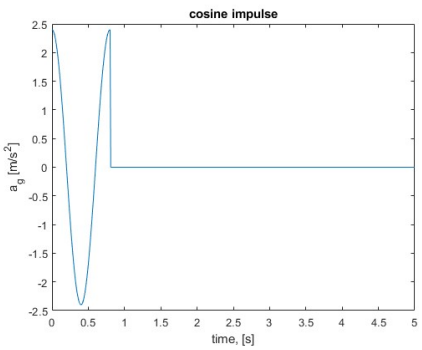

(**a**)

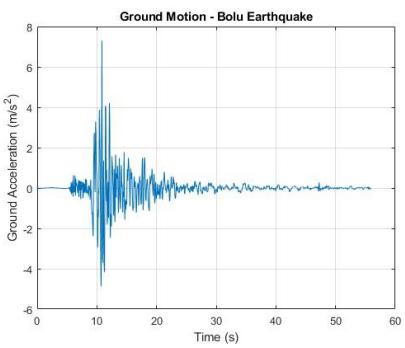

(**b**)

 doi:10.20944/preprints202603.1401.v1

Figure 3. cosine excitation and Turkey Bolu earthquake ground motion.

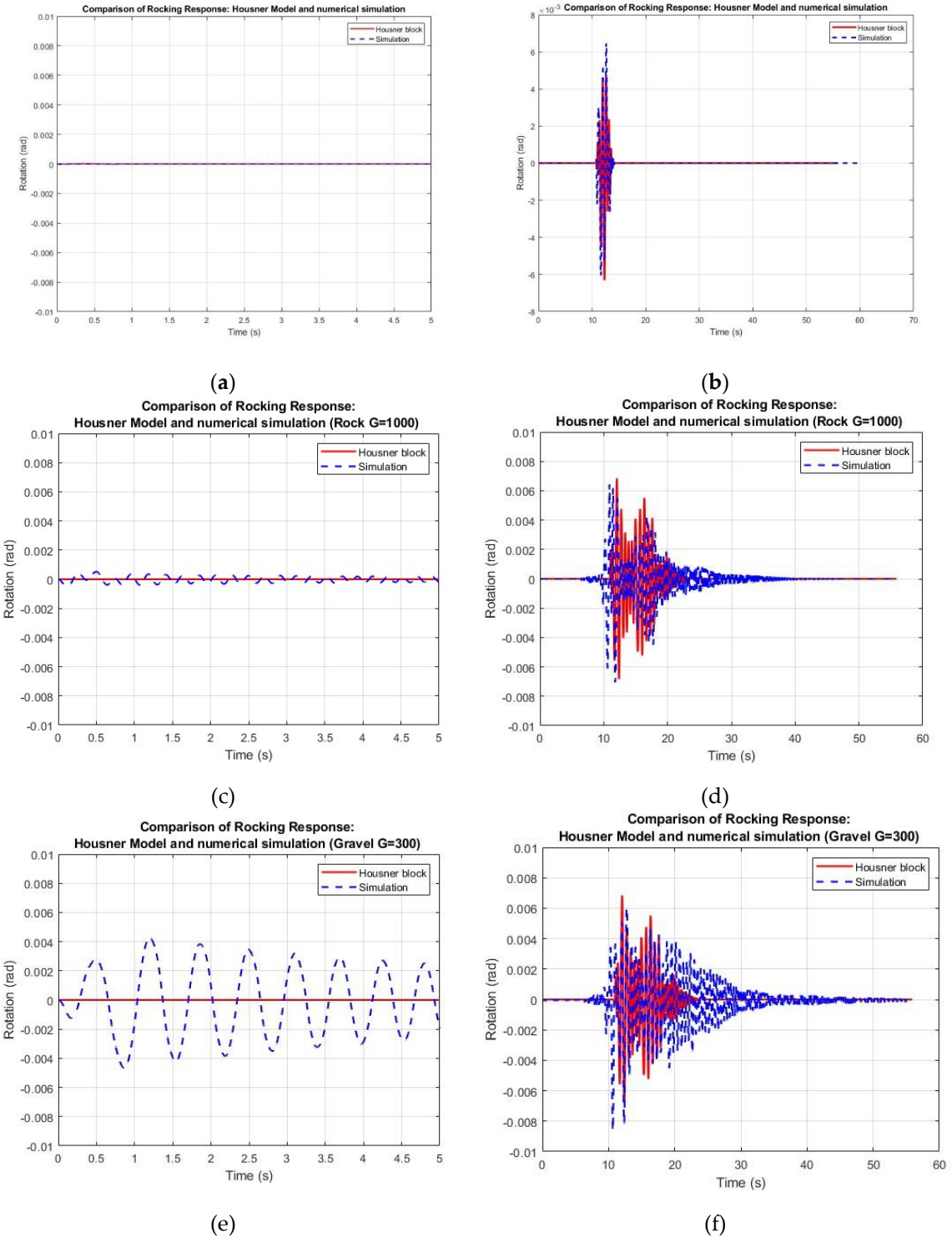

 doi:10.20944/preprints202603.1401.v1

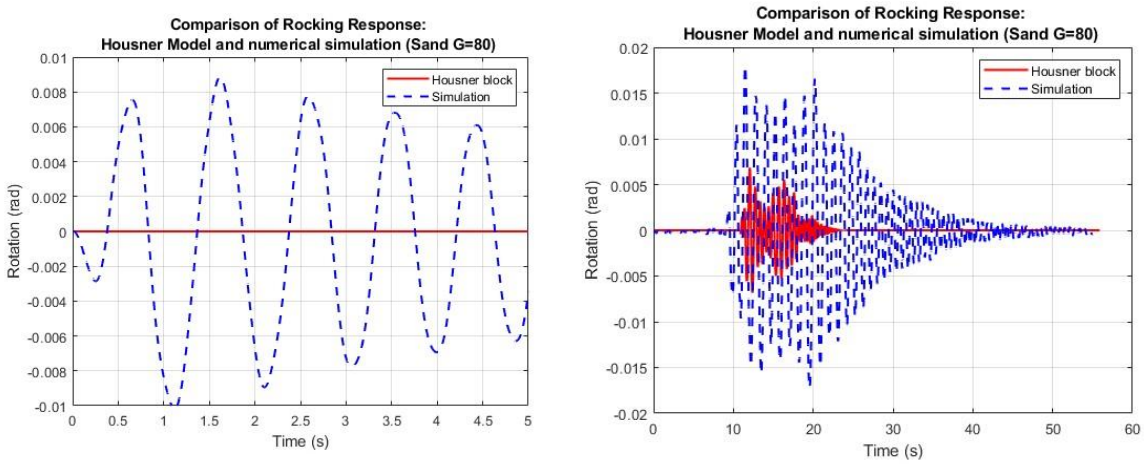

(g) (h)

Figure 4. Comparison of the Housner model and LS-DYNA simulations for rigid block rocking under cosine and earthquake excitations. Results are shown for four base materials: (4a,4b) Steel (E=210,000 MPa), (4c,4d) Rock (G=1,000 MPa), (4e,4f) Gravel (G=300 MPa), and (4g,4h) Sand (G=80 MPa).

3. Development of a Novel SSI-Rocking Model for Non-Anchored Structure on Compliant Base

In real-world scenarios, soil compliance plays a crucial role in structural rocking. A compliant base introduces additional vertical and rotational compliance, damping effects, and energy dissipation mechanisms, which can either enhance or impair stability. Experimental and numerical studies have shown that neglecting soil flexibility can lead to significant errors in predicting the overturning threshold and energy dissipation [23–27].

To address these limitations, we propose a novel SSI-rocking model that explicitly incorporates the elastic and damping properties of the soil. As shown in **Figure 5**, the model is formulated using the Lagrange method to capture the rocking behavior of structures on compliant foundations, improving upon classic rocking models by accounting for base flexibility. The proposed SSI-rocking model considers a two-degree-of-freedom (2-DOF) system subjected to ground excitation, where the structure's mass is idealized at its center. The system includes both rotational motion θ and translational motion to simulate base compliance effects. The base is modeled using frequency-dependent stiffness and damping characteristics, denoted as $K_v(\Omega)$ and $C_v(\Omega)$, respectively. The stiffness considered the soil flexibility and the contact stiffness between blocks and base. Energy dissipation due to inelastic impacts at the rocking edges is captured through an equivalent viscous damper, implemented as a dashpot. Unlike Housner's model, where damping occurs discontinuously only at the instant of impact, the proposed model features a viscous damper that operates continuously throughout the motion. Additionally, no plasticity or permanent deformation of the soil is considered. The Lagrange formulation is used to derive the equations of motion, incorporating both conservative forces, such as gravity and elastic restoring forces, and non-conservative effects, including damping and impact-induced energy losses.

Preprints.org (www.preprints.org) | NOT PEER-REVIEWED | Posted: 18 March 2026 doi:10.20944/preprints202603.1401.v1

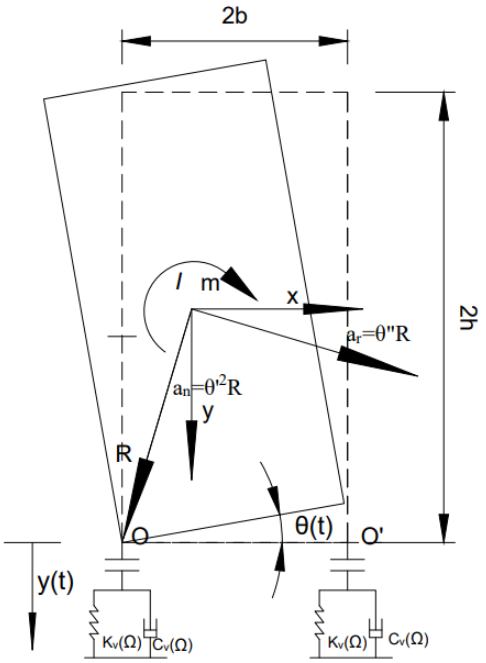

Figure 5. rocking block model on compliant base.

The rotational and vertical contributions to the system's kinetic energy are:

$$E_k = \frac{1}{2}I\dot{\theta}^2 + \frac{1}{2}m\left[\dot{y} + Rsin(\alpha sgn(\theta) - \theta)\dot{\theta}\right]^2 \quad (8)$$

The potential energy of the system is given, where the zero potential energy surface was defined at the pivot point of the rocking block.

$$E_p = \frac{1}{2}ky^2 + mg[Rcos(\alpha sgn(\theta) - \theta) - y] \quad (9)$$

The stiffness and damping properties are defined as follows:

$$\omega^2 = \frac{k}{m}\ ,\ 2\omega\xi = \frac{c}{m} \quad (10)$$

For non-conservative rocking system on compliant base, the Lagrange equation gives

$$\begin{aligned} \frac{d}{dt}\left(\frac{\partial L}{\partial \dot{\theta}}\right) - \frac{\partial L}{\partial \theta} &= Q(t) \\ \frac{d}{dt}\left(\frac{\partial L}{\partial \dot{y}}\right) - \frac{\partial L}{\partial y} &= c\dot{y} \end{aligned} \quad (11)$$

Combining Equations (7,8), the Lagrange Equations are simplified as follows:

$$(I + mR^2)\ddot{\theta} - mR^2\ddot{y}\sin(A) + mgRsin(A) = -m\ddot{u}_gRcos(A) \quad (12)$$

$$m\ddot{y} - mR\dot{\theta}\,sin\,(A) + mR\dot{\theta}\text{^}2\ cos\,(A) - (mg - ky) = -c\dot{y} \quad (13)$$

$$A(t) = sgn(\theta(t))\alpha - \theta(t), \qquad \gamma = R/g\ \rho\text{^}2, I = 4/3\ mR\text{^}2 \quad (14)$$

Combining Equations (11,12,13), the equation of motion of the rocking system on compliant base is derived:

 doi:10.20944/preprints202603.1401.v1

$$\ddot{y}(t) = \frac{\left(g - \omega^2 y - 2\omega\xi\dot{y} - R\cos(A)\dot{\theta}^2 + \frac{3}{7}\left(-\ddot{u}_g\cos(A)\sin(A) + g\sin(A)^2\right)\right)}{\left(1 - \frac{3}{7} * \sin^2(A)\right)} \tag{15}$$

$$\ddot{\theta}(t) = \frac{3}{7R}\left\{\left(\left(g - \omega^2 y - 2\omega\xi\dot{y} - R\cos(A)\dot{\theta}^2 + \frac{3}{7}\left(-\ddot{u}_g\cos(A)\sin(A) + g\sin(A)^2\right)\right)\left(1 - \frac{3}{7} * \sin^2(A)\right)\right)\sin(A) - g\sin(A) - \ddot{u}_g\cos(A)\right\} \tag{16}$$

Equation (14,15) can be solved numerically in MATLAB using ODE45.

4. Numerical Validation and Implementation

To validate the proposed analytical SSI-rocking model, the numerical simulations were implemented by using LS-DYNA. A calibration procedure was employed to optimize the interface stiffness parameter k by maximizing the Pearson correlation coefficient between the predictions of SSI-rocking model and the numerical simulation reference data. The objective was defined as

$$\theta^* = \arg\max_{\theta} \operatorname{corr}\left(y^{\text{ref}}(t), y^{\text{model}}(t,\theta)\right) \tag{17}$$

where $y^{\text{ref}}(t)$ represents the rotation time history from numerical simulation and $y^{\text{model}}(t,\theta)$ denotes the rocking angle computed by the SSI-rocking model. The correlation coefficient used for calibration was calculated as:

$$\operatorname{corr}\left(y^{\text{ref}}, y^{\text{model}}\right) = \frac{\sum_{i=1}^{N}\left(y_i^{\text{ref}} - \overline{y^{\text{ref}}}\right)\left(y_i^{\text{model}} - \overline{y^{\text{model}}}\right)}{\sqrt{\sum_{i=1}^{N}\left(y_i^{\text{ref}} - \overline{y^{\text{ref}}}\right)^2} \cdot \sqrt{\sum_{i=1}^{N}\left(y_i^{\text{model}} - \overline{y^{\text{model}}}\right)^2}} \tag{17}$$

where $\overline{y^{\text{ref}}}$ and $\overline{y^{\text{model}}}$ are the mean values of the reference data and estimated data from proposed model, respectively, and N is the number of data points. To ensure temporal alignment, the analytical model's output was interpolated to match the LS-DYNA time steps. A grid search was conducted over k_x values ranging from 1×10^5 *to* $9 \times 10^5\ kN/m$, with the equivalent damping ratio ξ ranging from 1% to 7%. For each k_x the rocking motion was solved using ODE45 solver, and the resulting $y^{\text{model}}(t,\theta)$ was compared to the simulation data $y^{\text{ref}}(t)$ to compute the correlation. The k_x yielding the highest correlation (above a threshold of 0.9) was selected, ensuring the analytical model accurately captures the dynamic rocking behavior observed in the numerical simulation. The close agreement between the calibrated analytical solution and numerical simulation **Figure 6**, as evidenced by the high correlation coefficient, validates the robustness of the proposed SSI-rocking model for predicting soil-structure interaction dynamics.

Figure 7 compares the seismic rocking response of a block (R = 9.39, α = 0.44) as predicted by the proposed SSI-rocking model, Housner's classical model, and LS-DYNA simulations. While Housner's model substantially underpredicts oscillation amplitudes due to its rigid-base assumption, the proposed analytical framework exhibits a close alignment with the high-fidelity numerical simulation. This high level of correlation demonstrates the model's precision in capturing complex dynamic responses on soft soil. Ultimately, these results underscore the superior reliability of the SSI-rocking model in incorporating critical soil-structure interaction effects, providing a more robust alternative for seismic stability assessments.

 doi:10.20944/preprints202603.1401.v1

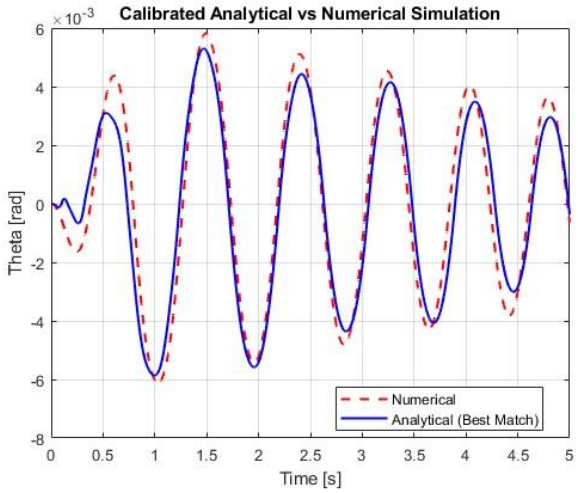

Figure 6. Verification of SSI-rocking model response for R = 9.39, α = 0.44. on Sand, $E = 280MPa, k = 3.95 * 10^8 N/m$.

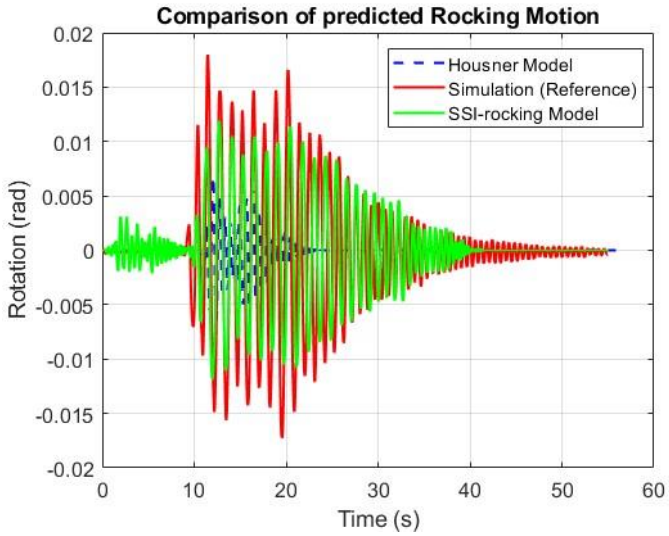

Figure 7. Comparison of predicted rocking motion of block R = 9.39, α = 0.44. under earthquake excitation: SSI-rocking model, Housner's model, and LS-DYNA simulation.

This investigation explores the influence of varying equivalent damping ratios (ξ = 0.01, 0.03, 0.05, 0.07) on the dynamic behavior of a structure subjected to controlled conditions (R = 5, R = 9, α = 1.2, k = 5×10⁸ N/m, **Figure 8**). The upper left chart depicts the rotational motion under a cosine function excitation, revealing that higher equivalent damping ratios markedly enhance the decay rate of oscillations. Notably, ξ = 0.07 demonstrates the most significant amplitude reduction, in contrast to ξ = 0.01, which sustains larger oscillations over a prolonged duration. The equivalent damping ratio also effectively mitigates rocking motion, with greater ξ values showing pronounced suppression. An equivalent damping ratio below 5% (ξ = 0.05) is recommended as an optimal threshold for the proposed SSI-rocking model. The upper right chart illustrates the vertical displacement over the same period, where an increase in the equivalent damping ratio similarly diminishes the amplitude of vertical motion and expedites the decay of oscillations, with ξ = 0.07 achieving the swiftest stabilization. Across these two charts, it is evident that, with a constant stiffness value, the equivalent damping ratio does not alter the rocking behavior of the blocks (R = 5 and R = 9), indicating a consistent structural response irrespective of the R value under these conditions. The stiffness plays a more significant role in rocking dynamics than damping.

 doi:10.20944/preprints202603.1401.v1

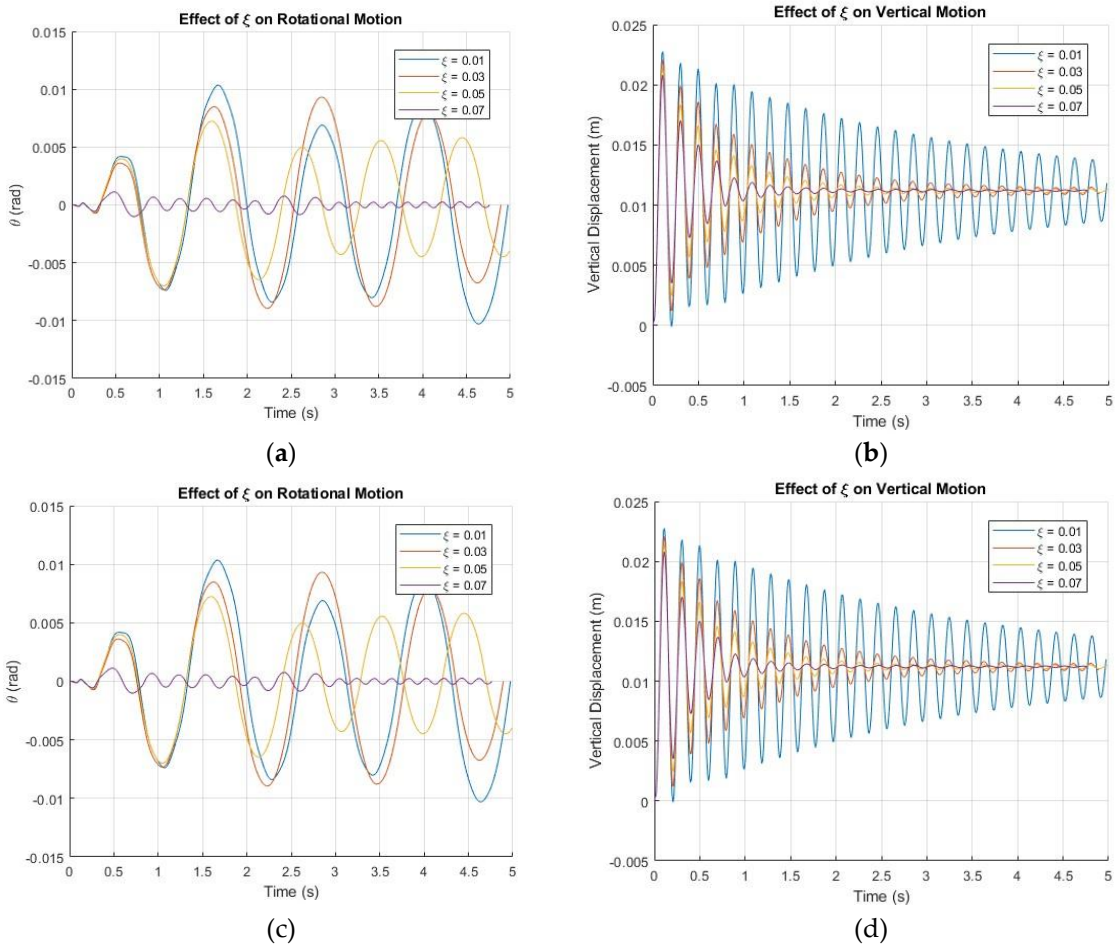

Figure 8. Damping Influence on Rotational and Vertical Motion of a block with R= 5 (8a,8b), R = 9 (8c,8d), with Stiffness (k = 5×10⁵ kN/m) and Varying Equivalent damping ratios (ξ = 0.01, 0.03, 0.05, 0.07).

5. The Effective Interface Stiffness for Rocking Motion

The effective interface stiffness of a rocking system is governed by four key parameters, including the Young's modulus (E) of the block, the Young's modulus of the underlying soil, the contact area of the block, and the effective depth of the soil domain. This effective interface stiffness plays a dominant role for rocking motion. To build a relationship between equivalent stiffness in proposed SSI-rocking model and the effective interface stiffness, we consider the combined deformability of both the block and the supporting soil.

The proposed stiffness relationship is formulated based on the concept of two elastic bodies in contact, where the overall response is determined by the harmonic sum of their respective stiffness contributions. The rocking effective interface stiffness k is expressed as:

$$k_{interface} = \frac{A}{H}\left[\frac{1}{\frac{1}{G_s}+\frac{1}{E_b}}\right] \tag{19}$$

Here, G_s represents the dynamic shear modulus of the soil, which governs its resistance to deformation under shear stress, while E_b is the Young's modulus of the block, characterizing its resistance to axial deformation. The term inside the brackets accounts for the combined compliance of both materials, treating the interface as a system of two springs in series. The fraction form reflects the inverse sum of their individual stiffness contributions, ensuring that the resulting stiffness captures both the flexibility of the soil and the rigidity of the block. The interface area A controls the distribution of contact stress between the block and the soil, H represents the depth of the soil that actively participates in the deformation process, effectively controlling the extent of the soil domain

 doi:10.20944/preprints202603.1401.v1

that contributes to the rocking response. A deeper soil domain implies a more compliant foundation, reducing the overall rocking stiffness. The ratio $\frac{A}{H}$ thus serves as a geometric scaling factor that adjusts the stiffness to account for both the extent of contact and the depth-dependent flexibility of the soil.

This formulation allows for an efficient estimation of the equivalent rocking interface stiffness, enabling the proposed SSI-rocking model to match numerical simulations more accurately. **Figure 9**. demonstrates the high fidelity of the calibrated SSI-rocking model against numerical simulations using the effective interface stiffness. The rotational time-history results confirm that the proposed analytical framework accurately captures the dynamic response on compliant foundations. Notably, the convergence with Housner's model for the steel-base case () further validates the model's consistency across the rigid-to-compliant spectrum.

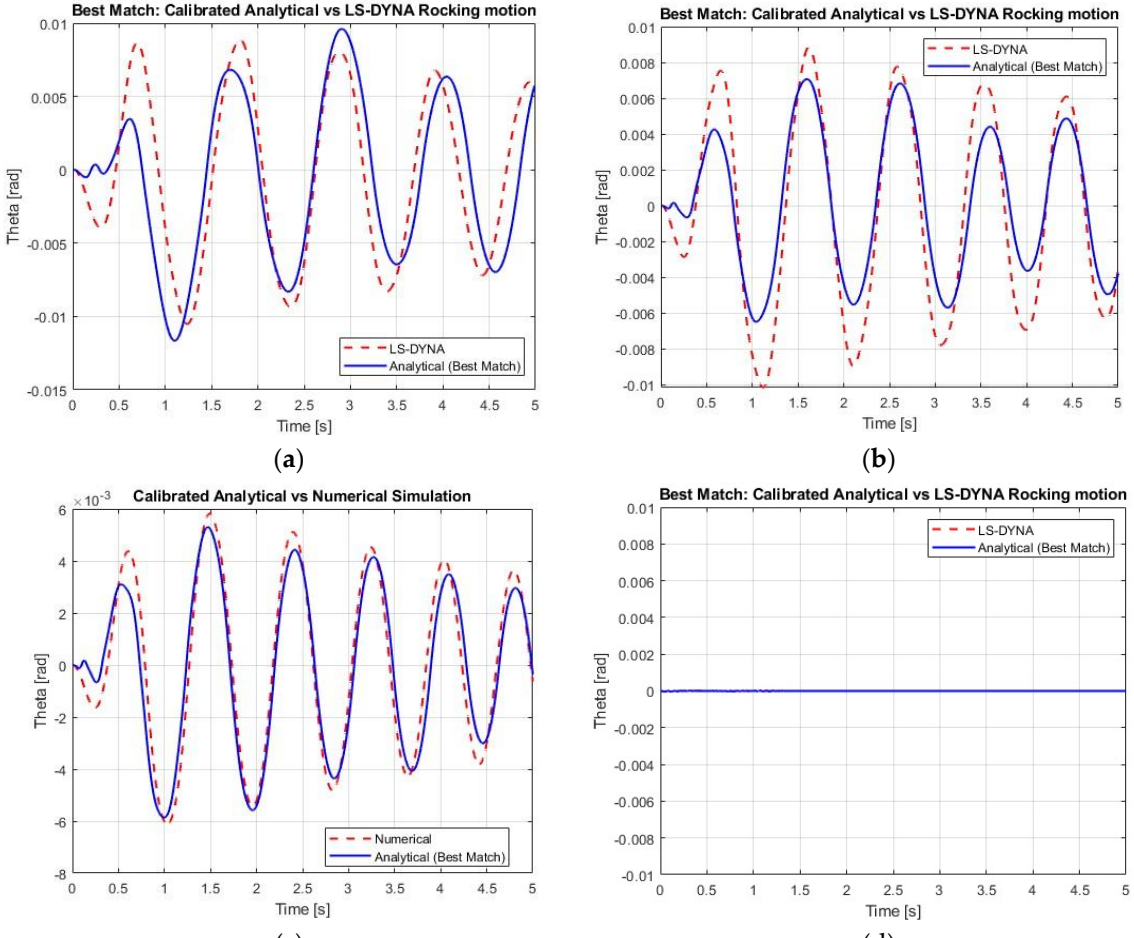

Figure 9. Verification of SSI-rocking model response for R = 9.39, α = 0.44. on Clay (9a) $E = 130MPa, k = 1 * 10^8 N/m$; on Sand (9b), $E = 280MPa, k = 3.95 * 10^8 N/m$; on Gravel (9c), $E = 525MPa, k = 5.5 * 10^8 N/m$; on steel base (9d), $E = 210000MPa, k = 5.5 * 10^8 N/m$;.

Influence of Soil Dynamic Shear Modulus G_s

Figure 10 illustrates the rotational response of a rocking block subjected to different soil conditions, characterized by varying elastic dynamic modulus (E_d). The cosine function (Figure 2) was used as input excitation. The results highlight the influence of soil stiffness on the rocking motion, with softer soils (e.g., clay, E = 130 MPa) exhibiting greater amplitudes and prolonged oscillations, while stiffer materials (e.g., steel, E = 210,000 MPa) significantly suppress rocking motion. This trend indicates that higher soil stiffness increases energy dissipation and reduces dynamic amplification effects. The observed phase shifts between various soil types provide additional

 doi:10.20944/preprints202603.1401.v1

evidence that the rocking period increases as subsoil stiffness decreases. Furthermore, the greater the flexibility of the soil, the larger the amplitude of the rocking motion might become.

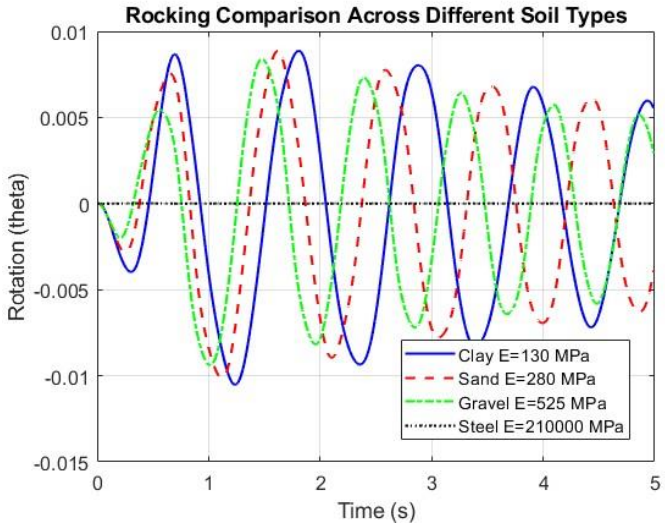

Figure 10. Rocking response over time for a rigid block R = 9.39, $\alpha = 0.44$. on four types of soil: sand (solid blue), clay (dashed red), gravel (dash-dot green), and silt (dotted black).

Influence of Block Elastic Modulus E_b

The influence of the block's Young's modulus on the rocking motion, as depicted in **Figure 11** varies across different soil types (clay, sand, gravel, and steel). The graphs compare the rotational response of a steel block (E = 210 GPa) and a concrete block (E = 30 GPa) under identical cosine excitation conditions on each soil type.

For softer soils like clay and sand, the block's E-modulus has a noticeable but relatively modest effect on the rocking motion. The steel and concrete blocks exhibit the same rocking amplitudes, while the rocking period of steel block compared to the concrete block increased slightly, indicating that a higher E-modulus (stiffer block) marginally enlarges the rocking period on a compliant base. On gravel, the difference becomes more pronounced. The rocking motion of steel block on gravel is considerably larger than the concrete block on gravel. On a very stiff base like steel, the rocking motion is heavily suppressed for both blocks, the cosine excitation was not strong enough to induce rocking. Overall, a higher block E-modulus (e.g., steel) tends to increase the amplitude and duration of rocking motion on a compliant base.

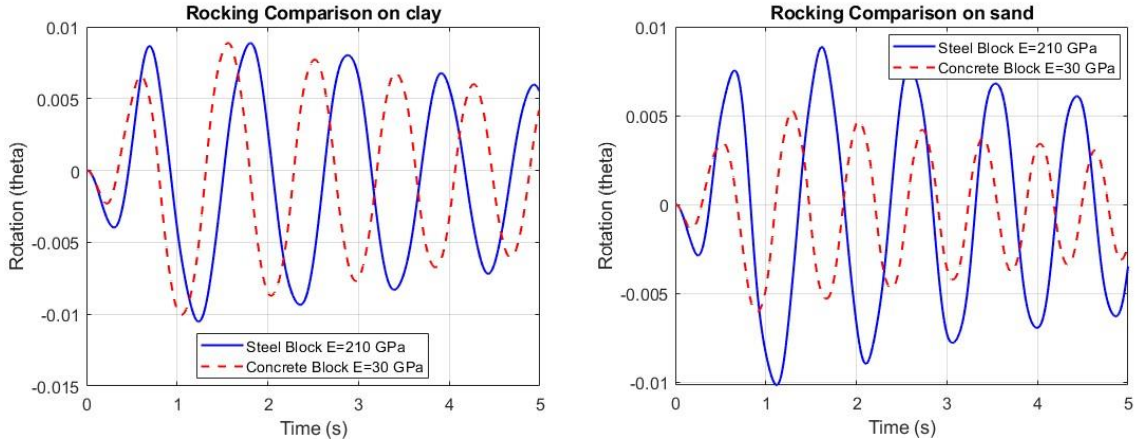

(**a**) (**b**)

 doi:10.20944/preprints202603.1401.v1

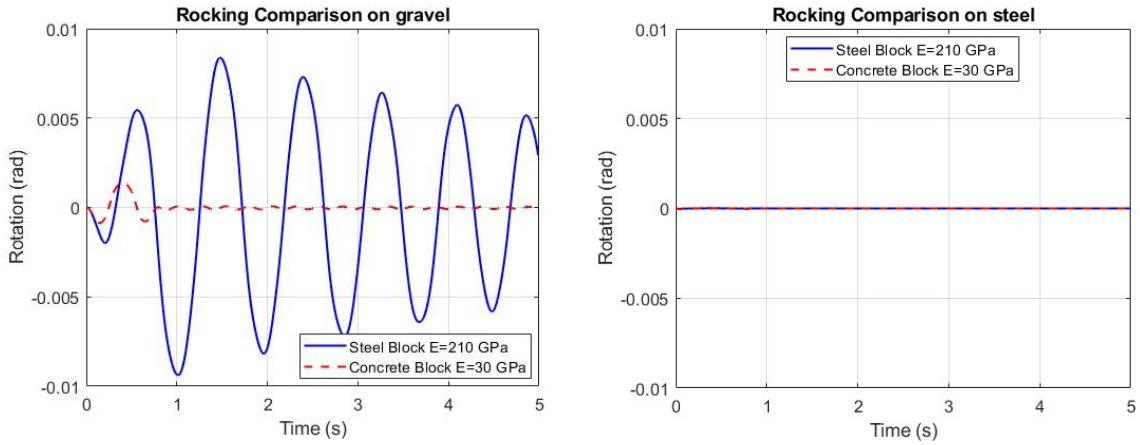

(c) (d)

Figure 11. Comparison of rocking response over time for steel and concrete blocks on clay $E = 130MPa$ (11a), sand $E = 280MPa$ (11b), gravel $E = 525MPa$ (11c), steel $E = 210000MPa$ (11d).

6. Conclusion

In conclusion, this study provides key insights into the behavior of rocking structures on softer subsoil bases, with the following points:

- The rocking initiation condition, defined as $a_g > gtan\alpha$ becomes significantly altered on a compliant base, particularly when the subsoil is softer than rock, rendering the classical Housner rigid block model inadequate.
- A novel SSI-rocking model, which considers soil-structure interaction, has been developed and thoroughly tested using LS-DYNA simulations, showing strong accuracy in predicting rocking motion on a flexible base.
- An effective interface stiffness has been introduced to fine-tune the SSI-rocking model. The relationship between equivalent stiffness and effective interface stiffness was studied.
- Soil stiffness plays a more critical role than damping in influencing rocking motion and softer soil may increase the likelihood of overturning.

Future studies could explore the application of the SSI-rocking model across a wider range of soil types—such as sandy, clayey, or layered profiles—and structural configurations, including varying geometries and masses, to further refine its predictive capabilities for seismic design. This could involve parametric analyses to assess the model's robustness under diverse geotechnical conditions and loading scenarios, potentially leading to standardized design guidelines for rocking structures on compliant bases.

Author Contributions: Writing – original draft, Visualization, Validation, Software, Methodology, Formal analysis, Data curation, Conceptualization, Investigation. B.Y; Writing – review & editing, Investigation, M.G; Writing – review & editing, Investigation, H.S.

Funding: This work was financially supported by the Deutsch Zentrum und Luft- und Raumfahrt (DLR), grant number IGF 22029.

Data Availability Statement: The data presented in this study are available on request from this corresponding author due to privacy.

Acknowledgments: The authors would like to acknowledge the use of DeepL and Gemini (Google) for linguistic editing and structural refinement of this manuscript. These tools were utilized solely to enhance the clarity and readability of the text; all technical content, original derivations, and concluding interpretations remain the sole responsibility of the authors.

Conflicts of Interest: The authors declare that they have no known competing financial interests.

 doi:10.20944/preprints202603.1401.v1

References

1. M. Groß and H. Sadegh-Azar, "Damping approaches in nonlinear seismic time history analysis for large mobile equipment with uplift," Oct. 24, 2023, Wiley. doi: 10.1002/stco.202200049.
2. M. Groß, D. Gaube, and H. Sadegh-Azar, "Grundsätzliche Untersuchungen zum seismischen Verhalten schienengebundener mobiler Großgeräte der Fördertechnik Teil 2: Seismische Analysen und Validierung." 2021.
3. M. Groß, D. Gaube, and H. Sadegh-Azar, "Grundsätzliche Untersuchungen zum seismischen Verhalten schienengebundener mobiler Großgeräte der Fördertechnik Teil 1: Stand der Technik und Berechnungsansätze." 2021.
4. G. W. Housner, "The behavior of inverted pendulum structures during earthquakes," Feb. 01, 1963, Seismological Society of America. doi: 10.1785/bssa0530020403.
5. C. Yim, A. K. Chopra, and J. Penzien, "Rocking response of rigid blocks to earthquakes," Jan. 01, 1980, Wiley. doi: 10.1002/eqe.4290080606.
6. J. Zhang and N. Makris, "Rocking Response of Free-Standing Blocks under Cycloidal Pulses," May 01, 2001, American Society of Civil Engineers. doi: 10.1061/(asce)0733-9399(2001)127:5(473).
7. M. A. ElGawady, Q. Ma, J. Butterworth, and J. Ingham, "Effects of interface material on the performance of free rocking blocks," Jul. 21, 2010, Wiley. doi: 10.1002/eqe.1025.
8. E. G. Dimitrakopoulos and M. J. DeJong, "Overturning of Retrofitted Rocking Structures under Pulse-Type Excitations," Feb. 11, 2012, American Society of Civil Engineers. doi: 10.1061/(asce)em.1943-7889.0000410.
9. M. J. DeJong and E. G. Dimitrakopoulos, "Dynamically equivalent rocking structures," Feb. 10, 2014, Wiley. doi: 10.1002/eqe.2410.
10. M. F. Vassiliou and N. Makris, "Estimating Time Scales and Length Scales in Pulselike Earthquake Acceleration Records with Wavelet Analysis," Mar. 22, 2011, Seismological Society of America. doi: 10.1785/0120090387.
11. M. F. Vassiliou, K. R. Mackie, and B. Stojadinović, "A finite element model for seismic response analysis of deformable rocking frames," Aug. 23, 2016, Wiley. doi: 10.1002/eqe.2799.
12. M. F. Vassiliou, R. Truniger, and B. Stojadinović, "An analytical model of a deformable cantilever structure rocking on a rigid surface: development and verification," Jul. 30, 2015, Wiley. doi: 10.1002/eqe.2608.
13. J. A. Bachmann, M. F. Vassiliou, and B. Stojadinović, "Dynamics of rocking podium structures," May 23, 2017, Wiley. doi: 10.1002/eqe.2915.
14. J. A. Bachmann, M. F. Vassiliou, and B. Stojadinović, "Rolling and rocking of rigid uplifting structures," Aug. 19, 2019, Wiley. doi: 10.1002/eqe.3213.
15. J. A. Bachmann, M. K. Strand, M. F. Vassiliou, M. Broccardo, and B. Stojadinović, "Is rocking motion predictable?," Oct. 05, 2017, Wiley. doi: 10.1002/eqe.2978.
16. C. G. Lachanas, D. Vamvatsikos, and M. F. Vassiliou, "The influence of the vertical component of ground motion on the probabilistic treatment of the rocking response of free-standing blocks," Mar. 20, 2022, Wiley. doi: 10.1002/eqe.3643.
17. N. R. Manzo, C. G. Lachanas, M. F. Vassiliou, and D. Vamvatsikos, "Uniform risk spectra for rocking structures," Jun. 09, 2022, Wiley. doi: 10.1002/eqe.3691.
18. N. R. Manzo and M. F. Vassiliou, "Displacement-based analysis and design of rocking structures," Sep. 02, 2019, Wiley. doi: 10.1002/eqe.3217.
19. M. Sieber, M. F. Vassiliou, and I. Anastasopoulos, "Intensity measures, fragility analysis and dimensionality reduction of rocking under far-field ground motions," Oct. 05, 2022, Wiley. doi: 10.1002/eqe.3740.
20. A. K. Kazantzi, C. G. Lachanas, and D. Vamvatsikos, "Seismic response distribution expressions for on-ground rigid rocking blocks under ordinary ground motions," Jul. 06, 2021, Wiley. doi: 10.1002/eqe.3511.
21. C. G. Lachanas, D. Vamvatsikos, and E. G. Dimitrakopoulos, "Statistical property parameterization of simple rocking block response," Oct. 24, 2022, Wiley. doi: 10.1002/eqe.3765.
22. C. G. Lachanas and D. Vamvatsikos, "Rocking incremental dynamic analysis," Dec. 13, 2021, Wiley. doi: 10.1002/eqe.3586.

 doi:10.20944/preprints202603.1401.v1

23. A. Palmeri and N. Makris, "Response analysis of rigid structures rocking on viscoelastic foundation," Mar. 17, 2008, Wiley. doi: 10.1002/eqe.800.
24. M. F. Vassiliou and N. Makris, "Analysis of the rocking response of rigid blocks standing free on a seismically isolated base," Apr. 08, 2011, Wiley. doi: 10.1002/eqe.1124.
25. I. Pelekis, S. Madabhushi, and M. J. DeJong, "Soil behaviour beneath buildings with structural and foundation rocking," May 01, 2019, Elsevier BV. doi: 10.1016/j.soildyn.2019.04.012.
26.] I. Pelekis, S. Madabhushi, and M. J. DeJong, "Seismic performance of buildings with structural and foundation rocking in centrifuge testing," Jul. 19, 2018, Wiley. doi: 10.1002/eqe.3089.
27. Y. Lu, F. Xiong, and Q. Ge, "Dynamic rocking response of a rigid planar block on a nonlinear hysteretic Winkler foundation," May 22, 2021, Wiley. doi: 10.1002/eqe.3470.
28. D. He, P. Li, and Z. Zhang, "Analysis of a Simplified Model of a Rigid Rocking Block on Winkler Foundation," Mar. 13, 2023, Multidisciplinary Digital Publishing Institute. doi: 10.3390/su15065095.
29. P. Frost and P. Cacciola, "Rocking of rigid blocks standing on a horizontally-moving compliant base," Apr. 11, 2023, Elsevier BV. doi: 10.1016/j.ijnonlinmec.2023.104416.
30. Arbeitskreis Baugrunddynamik, "Empfehlungen des Arbeitskreises Baugrunddynamik," Herausgegeben von der Deutschen Gesellschaft für Geotechnik e.V. (DGGT), 2019.